Ultralow lattice thermal conductivity in Tl-based chalcogenides via rattling-driven phonon localization

Nidheesh Virakante, Rajan Kumar, and Ankit Jain*
Mechanical Engineering Department, Indian Institute of Technology Bombay, Mumbai 400076, India

(Received 8 May 2026; accepted 26 June 2026; published 15 July 2026)

Materials with ultralow lattice thermal conductivity (LTC) are of fundamental and technological importance for thermal management and thermoelectric energy conversion, yet identifying crystalline solids that intrinsically suppress heat transport remains challenging. Here, we present a comprehensive first-principles investigation of lattice thermal transport in the tetragonal chalcogenides $Tl_2CdSnTe_4$, $Tl_2CdGeTe_4$, and $Tl_2HgSnSe_4$. By integrating temperature-dependent effective potential theory, anharmonic phonon renormalization, four-phonon scattering, and the multichannel transport formalism, we predict exceptionally low in-plane LTC values of 0.32, 0.30, and 0.29 $W\,m^{-1}\,K^{-1}$ at 300 K, placing these materials among the lowest reported for bulk inorganic crystals. The ultralow thermal transport originates from pronounced rattling dynamics of Tl atoms, which induce localization of low-frequency vibrational modes and strongly suppress heat-carrying acoustic phonons. Beyond conventional particlelike transport, coherent contributions become increasingly important at elevated temperatures, leading to a weak temperature dependence of LTC. We further show that tensile strain enhances anharmonicity and reduces LTC, while mass perturbation via isovalent substitution yields additional suppression through enhanced phonon scattering, reaching 0.16 $W\,m^{-1}\,K^{-1}$ under 1% strain. These results establish Tl-based chalcogenides as a promising class of intrinsically ultralow-LTC materials and highlight the effectiveness of combining heavy-atom rattling, strain, and compositional tuning for phonon engineering in these materials.

DOI: 10.1103/wh1q-59bc

I. INTRODUCTION

Reducing lattice thermal conductivity (LTC) is central to the development of advanced thermal insulation and high-efficiency thermoelectric materials [1–3]. In crystalline solids, heat is predominantly carried by phonons, and its suppression requires disrupting phonon propagation through enhanced scattering, reduced group velocities, and/or loss of coherence [4–7]. Materials exhibiting ultralow LTC typically possess complex unit cells, structural disorder, weakly bonded sublattices, or loosely bound "rattler" atoms that introduce strong anharmonicity and phonon localization [8–15]. Despite extensive research efforts, most materials with LTC below 0.5 $W\,m^{-1}\,K^{-1}$ are either structurally complex or weakly bonded, limiting their practical utility [16]. Identifying simple, chemically stable, three-dimensional crystalline materials with intrinsically suppressed phonon transport, therefore, remains an important challenge [16].

Rattler-induced phonon scattering has emerged as a particularly effective route to suppress LTC [17–19]. In a range of halides, chalcogenides, and cagelike systems, heavy atoms occupying oversized coordination environments exhibit large-amplitude, anharmonic vibrations that hybridize with acoustic phonons, generating localized modes and strong scattering [19–21]. This interaction can significantly reduce phonon lifetimes and, in some cases, drive a crossover toward glasslike thermal transport. Tl-containing compounds are especially promising in this regard, as stereochemically active lone pairs and weak bonding environments promote pronounced anharmonic dynamics [16,22–26]. Promising compounds that are reported to have Tl-rattling-induced ultralow LTC include $AgTlI_2$ [16], Tl_3VSe_4 [27], and $TlInTe_2$ [23], with room temperature LTCs of 0.25, 0.30, and 0.40 $W\,m^{-1}\,K^{-1}$ respectively.

Here, we investigate lattice thermal transport in the quaternary semiconductors $Tl_2CdSnTe_4$, $Tl_2CdGeTe_4$, and $Tl_2HgSnSe_4$. By screening the Materials Project database [28], we identified these compounds as stable, nonmagnetic semiconductors suitable for predictive first-principles analysis. Since the conventional phonon transport theory was previously shown to be inadequate for describing thermal transport in strongly anharmonic and ultralow-LTC material systems, we employ a comprehensive computational framework that integrates temperature-dependent effective potential theory, anharmonic phonon renormalization, four-phonon scattering, and a multichannel thermal transport formalism. This enables a unified description of both particlelike and wavelike heat conduction beyond the conventional Boltzmann transport approach [29–32].

We show that these materials exhibit exceptionally low LTC, originating from pronounced rattling dynamics of Tl atoms that induce strong localization of low-frequency vibrational modes and suppress heat-carrying acoustic phonons. Notably, coherent (wavelike) phonon transport becomes increasingly significant at elevated temperatures, highlighting the breakdown of a purely particle-based description. We further demonstrate that tensile strain enhances anharmonic

*Contact author: a_jain@iitb.ac.in

 ©2026 American Physical Society

interactions, thereby further suppressing LTC. Finally, leveraging the shared structural and vibrational characteristics of these compounds, we identify design strategies to selectively suppress the particlelike transport channel, enabling further reduction of LTC to $0.16\,\mathrm{W\,m^{-1}\,K^{-1}}$ in $Tl_4Cd_2SnGeTe_8$ at 300 K under 1% tensile strain.

II. COMPUTATIONAL METHODOLOGY

The total phonon-mediated LTC κ^t is obtained by summing up contributions from particle channels (κ^p, also referred to as the population channel) and wavelike coherent channels (κ^c) as [29,31,33]

$$\kappa^t = \kappa^p + \kappa^c. \tag{1}$$

The contribution from the particle channel is obtained using the Peirls-Boltzmann transport equation [29,34], and that from the coherent channel is evaluated from the Wigner formalism [31]. The particle-channel LTC in the α direction, for an applied heat flux in the β direction, is given by [4,35]

$$\kappa^p_{\alpha\beta} = \sum_{\boldsymbol{q}} \sum_{\nu} c_{\boldsymbol{q}\nu} v_{\boldsymbol{q}\nu,\alpha} v_{\boldsymbol{q}\nu,\beta} \tau_{\boldsymbol{q}\nu,\alpha}, \tag{2}$$

where c, v, and τ are the phonon volumetric specific heat, group velocity, and scattering time, respectively, and the summation is over all the phonon modes with wave vector $\boldsymbol{q}$ and polarization ν. The coherent-channel LTC is given by [31,33]

$$\kappa^c_{\alpha\beta} = \frac{\hbar^2}{k_B T^2} \frac{1}{VN} \sum_{\boldsymbol{q}} \sum_{(\nu \neq \nu_1)} \frac{\omega_{\boldsymbol{q}\nu} + \omega_{\boldsymbol{q}\nu_1}}{2} V^{\alpha}_{\boldsymbol{q},\nu\nu_1} V^{\beta}_{\boldsymbol{q},\nu_1\nu} \times \frac{\omega_{\boldsymbol{q}\nu} n_{\boldsymbol{q}\nu}(n_{\boldsymbol{q}\nu}+1) + \omega_{\boldsymbol{q}\nu_1} n_{\boldsymbol{q}\nu_1}(n_{\boldsymbol{q}\nu_1}+1)}{4(\omega_{\boldsymbol{q}\nu} - \omega_{\boldsymbol{q}\nu_1})^2 + (\Gamma_{\boldsymbol{q}\nu} + \Gamma_{\boldsymbol{q}\nu_1})^2} (\Gamma_{\boldsymbol{q}\nu} + \Gamma_{\boldsymbol{q}\nu_1}), \tag{3}$$

where $\hbar$ is the reduced Planck constant, k_B is the Boltzmann constant, T is the temperature, V is the unit cell volume, N is the number of $\boldsymbol{q}$ points, ω is the phonon frequency, n is the Bose-Einstein distribution ($n_{\boldsymbol{q}\nu} = \frac{1}{e^x - 1}$, with $x = \frac{\hbar\omega_{\boldsymbol{q}\nu}}{k_B T}$), Γ is the phonon linewidth ($\Gamma_{\boldsymbol{q}\nu} = 1/\tau_{\boldsymbol{q}\nu}$), and $V^{\alpha}_{\boldsymbol{q},\nu\nu_1}$ is the α component of the velocity operator. Further details regarding these calculations can be found elsewhere [29,31,34].

The temperature-dependent cubic and quartic interatomic force constants (IFCs) are obtained by simultaneously fitting them to the force-displacement dataset obtained from density functional theory (DFT) [36,37] calculations for thermally perturbed supercells [30]. This method applies thermal displacements to atoms in the supercell according to the phonon spectrum and desired temperature [29,30]. Further, quartic renormalization of the phonon frequencies is carried out to incorporate the effect of anharmonicity in the phonon frequencies [29,30]. Subsequently, the higher-order four-phonon scattering channel is also included to accurately capture the phonon thermal transport in anharmonic materials [24,29,38].

The plane-wave-based DFT calculations are performed using the quantum mechanical package quantum espresso [39,40] employing Perdew-Burke-Ernzerhof revised for solids (PBEsol) exchange correlation functionals [41] with optimized norm-conserving Vanderbilt pseudopotentials [42]. The choice of PBEsol over the conventionally used Perdew-Burke-Ernzerhof (PBE) functional is motivated by the benchmark study by Srivastava *et al.*, in which the authors reported underprediction of thermal conductivity in a wide range of crystalline materials using PBE functionals [43]. The plane-wave energy cutoff and electronic wave vector grid are set at 100 Ry and $4 \times 4 \times 4$. The bare (i.e., temperature-independent) harmonic IFCs are obtained using density functional perturbation theory (DFPT) [44,45] calculations, which employ a primitive unit cell and the same phonon wave vector grid as that used for electrons. The Born effective charges and dielectric constant are also obtained using the DFPT calculations to account for long-range ionic interactions. The phonon wave vector grid is later interpolated in phonon scattering rate calculations to $12 \times 12 \times 12$. The temperature-dependent higher-order IFCs are evaluated using a Taylor series fitting approach to the force-displacement data on supercells. The phonon eigenmodes are used to give thermal displacements (corresponding to desired temperatures) to atoms in the supercells, and the interatomic forces on these supercells are obtained using DFT with Γ-point sampling of the electronic Brillouin zone. The third- and fourth-order IFCs are simultaneously evaluated by fitting the force-displacement data corresponding to 200 thermally perturbed supercells, each with $3 \times 3 \times 3$ repetitions of the eight-atom primitive unit cell, resulting in a total of 216 atoms per supercell. The cubic and quartic interaction cutoffs are set at 7.0 and 4.0 Å for third- and fourth-order IFCs. Phonon renormalization [30] of the second-order IFCs and subsequent updating of the third- and fourth-order IFCs are carried out iteratively until convergence is achieved (less than 2% change in harmonic IFCs in subsequent iterations). The computationally expensive four-phonon calculations are made tractable using the stochastic sampling computational approach proposed in Refs. [46,47]. All phonon scattering and LTC calculations are carried out using our in–house code [29,34,43].

III. RESULTS

A. Materials screening and structural stability

To identify Tl-based compounds with the potential for intrinsically low LTC, we screened the Materials Project database [28] for experimentally reported quaternary semiconductors containing Tl. The selection criteria included thermodynamic stability (energy above the convex hull <10 meV/atom), a finite electronic band gap (>0.25 eV), a nonmagnetic ground state, and a moderate unit cell size ($\leqslant 20$ atoms), yielding three candidate compounds: $Tl_2CdSnTe_4$, $Tl_2CdGeTe_4$, and $Tl_2HgSnSe_4$. All three compounds crystallize in a tetragonal structure with space group $I\bar{4}2m$ (No. 121) and contain eight atoms in the primitive unit cell. Fully relaxed structures and harmonic phonon dispersion calculations confirm their dynamical stability, as evidenced by the absence of imaginary phonon modes, and are thus considered for detailed thermal transport analysis.

The crystal structure of $Tl_2CdSnTe_4$ is shown in Fig. 1; $Tl_2CdGeTe_4$ (Ge substituted at the Sn site) and $Tl_2HgSnSe_4$ (Hg and Se substituted at the Cd and Te sites, respectively) adopt the same structural framework. All three compounds are

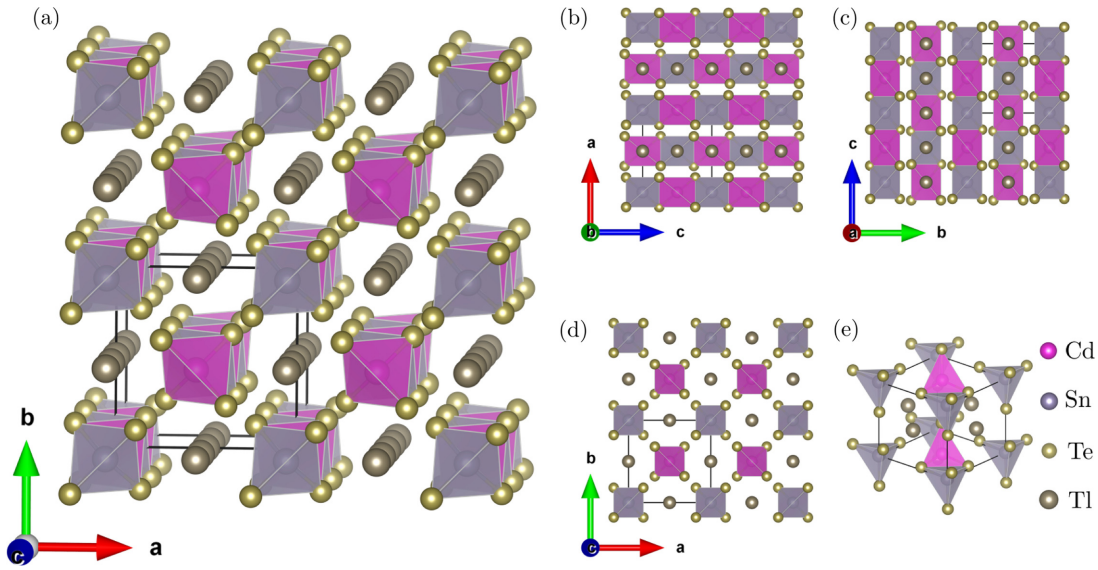


FIG. 1. Crystal structure of $Tl_2CdSnTe_4$. (a) Arrangement of Tl chains and edge-sharing Cd/Sn-Te_4 tetrahedra along the cross-plane (c-axis) direction shown in a $2 \times 2 \times 2$ supercell; the conventional unit cell is highlighted in black. Orthogonal projections of the same supercell in the (b) ac, (c) bc, and (d) ab planes. (e) The primitive unit cell (eight atoms) employed in the calculations, with atomic labeling.

structurally related to $TlInTe_2$, which exhibits an in-plane LTC of $\sim 0.40\,W\,m^{-1}\,K^{-1}$ at 300 K [23,25,48]. In this structure, the In sublattice is replaced by Cd/Sn (or Cd/Ge and Hg/Sn), giving rise to quaternary analogs while preserving the underlying topology.

The structure consists of alternating Cd-Sn and Tl chains along the cross-plane direction [Fig. 1(a)]. Each Cd and Sn atom is tetrahedrally coordinated by Te atoms, forming edge-sharing Cd- and Sn-centered tetrahedra that extend along the cross-plane direction, resulting in an anisotropic framework. In contrast, Tl atoms are coordinated by eight Te atoms in a square antiprismatic environment, forming oversized cages with relatively weak bonding. This environment facilitates large-amplitude Tl vibrations, consistent with rattling dynamics that are expected to strongly influence phonon transport. Similar structural and coordination features are present in $Tl_2CdGeTe_4$ and $Tl_2HgSnSe_4$.

The relaxed lattice parameters obtained from DFT at 0 K are $a = b = 8.39$ Å and $c = 7.11$ Å for $Tl_2CdSnTe_4$, $a = b = 8.33$ Å and $c = 7.00$ Å for $Tl_2CdGeTe_4$, and $a = b = 7.96$ Å and $c = 6.86$ Å for $Tl_2HgSnSe_4$, in good agreement with available experimental values (8.42 and 7.22 Å, 8.38 and 7.07 Å, and 8.04 and 6.89 Å, respectively) [49,50]. The slight underestimation of the lattice parameters (<1.5%) is addressed by examining thermal transport under tensile strain.

B. Phonon dispersion

The temperature-dependent phonon dispersions of $Tl_2CdSnTe_4$ along high-symmetry directions for temperatures ranging from 100 to 500 K are presented in Fig. 2(a) [refer to Figs. S2 and S3 in the Supplemental Material (SM) [51] for $Tl_2CdGeTe_4$ and $Tl_2HgSnSe_4$]. With increasing temperature, anharmonic renormalization induces moderate stiffening of low-frequency acoustic and optical modes, whereas high-frequency optical branches remain largely unaffected. For instance, the lowest acoustic mode at the X point hardens by ∼10%, 11%, and 29% in $Tl_2CdSnTe_4$, $Tl_2CdGeTe_4$, and $Tl_2HgSnSe_4$, respectively, between 100 and 500 K, whereas the highest optical modes change by less than 1%. These trends indicate that anharmonic interactions predominantly affect low-energy phonons, which play a central role in heat transport.

The partial phonon density of states at 300 K [Fig. 2(a), right panel] indicates that Tl atoms dominate the vibrational spectrum of low-energy phonons (i.e., below 2 THz), overlapping strongly with heat-carrying acoustic branches. These Tl-dominated low-frequency modes are therefore expected to play an important role in governing lattice thermal transport. Consistent with the strong anharmonic renormalization of these modes, the direction-resolved mean-square displacements (MSDs) shown in Fig. 2(b) are substantially large for Tl atoms, reflecting the weak bonding of Tl atoms, in both the in-plane (ab-plane) and cross-plane (c-plane) directions. Furthermore, the phonon participation ratios presented in Fig. 2(c) suggest that these Tl-dominated modes are highly localized, indicating pronounced rattling behavior and associated phonon localization. While Cd atoms exhibit comparable in-plane MSDs in $Tl_2CdSnTe_4$ and $Tl_2CdGeTe_4$, their contribution to low-frequency heat-carrying modes is minimal, whereas Hg atoms in $Tl_2HgSnSe_4$ contribute more significantly, albeit less than Tl atoms.

A pronounced anisotropy is observed between the in-plane (Γ-X-M) and out-of-plane (Γ-Z) phonon dispersions in all three compounds. Along the in-plane directions, the low-frequency acoustic branches exhibit frequent avoided crossings and strong distortions due to hybridization with Tl-dominated localized modes. This enhanced mode mixing reflects stronger coupling between Tl rattling vibrations and framework phonons within the ab plane. This interaction reduces group velocities and enhances phonon scattering, leading to significant suppression of in-plane heat transport. In contrast, the corresponding branches along Γ-Z retain comparatively smoother dispersions and weaker

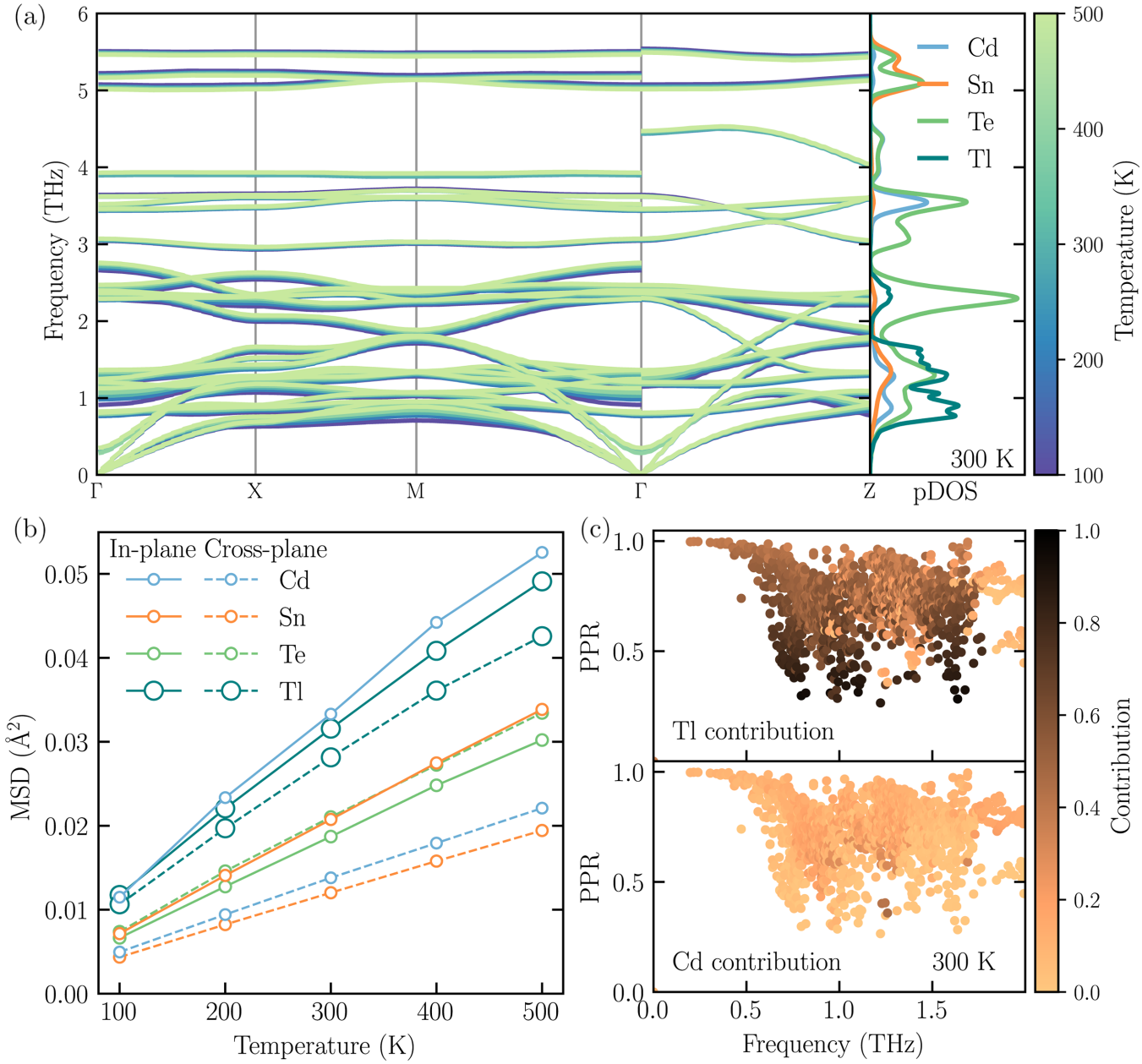


FIG. 2. Harmonic phonon properties of $Tl_2CdSnTe_4$. (a) Temperature-dependent phonon dispersions along high-symmetry directions from 100 to 500 K, together with the atom-projected partial density of states (pDOS) at 300 K. (b) Temperature-dependent mean-square displacements (MSDs) along the in-plane and cross-plane directions; marker sizes are scaled by atomic number. (c) Phonon participation ratios (PPRs) at 300 K for frequencies up to 2 THz, along with the contributions of Tl and Cd atoms to these modes. Corresponding results for $Tl_2CdGeTe_4$ and $Tl_2HgSnSe_4$ are provided in Figs. S2 and S3 of the Supplemental Material [51].

hybridization, indicating reduced coupling between Tl vibrations and out-of-plane phonons. This behavior can be attributed to the quasi-one-dimensional chainlike arrangement of Tl atoms along the *c* axis and leads to more severe degradation of phonon transport in the in-plane direction than along the *c* axis, consistent with the observed lower in-plane LTC in all three materials (discussed later). The directional dependence of phonon hybridization is further supported by the temperature-dependent MSDs shown in Fig. 2(b). In all three compounds, the in-plane MSDs are consistently larger than the corresponding cross-plane values, indicating stronger vibrational amplitudes within the *ab* plane.

C. Lattice thermal conductivity

The temperature-dependent LTCs of all three compounds in the in-plane and cross-plane directions obtained within the full multichannel thermal transport framework (LTCs obtained by considering different transport theory physics are reported in Tables S1 to S3 in the SM [51]) are summarized in Fig. 3(a). The inclusion of phonon renormalization is found to significantly enhance the predicted LTCs in these materials (a more than 33% increase in the in-plane LTC at 300 K), whereas the higher-order four-phonon scattering events are found to minimally suppress the thermal

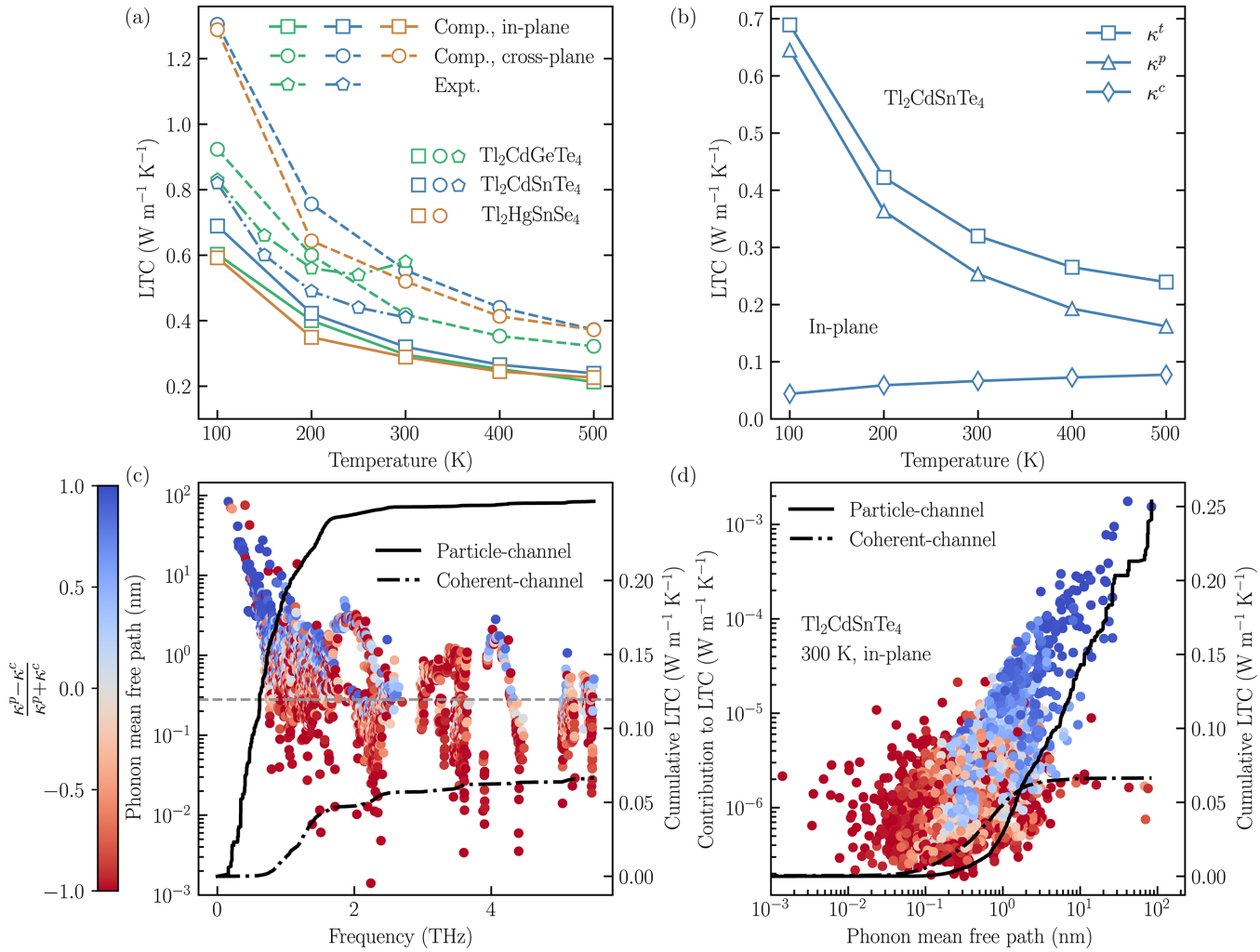


FIG. 3. Lattice thermal conductivity of Tl-based chalcogenides. (a) Temperature-dependent lattice thermal conductivity (LTC) along the in-plane and cross-plane directions for all three compounds; available experimental data (direction-averaged values on polycrystalline pellets) are taken from Ref. [49]. (b) Temperature-dependent decomposition of the in-plane LTC κ^t of $Tl_2CdSnTe_4$ into particle (κ^p) and coherent (κ^c) contributions. (c) Mode-resolved phonon mean free paths (primary y axis) and cumulative in-plane LTC (secondary y axis) as a function of phonon frequency at 300 K. The dashed horizontal line on the primary y axis corresponds to the Ioffe-Regel limit (corresponding to the minimum interatomic distance in the material). (d) Mode-resolved contributions to the in-plane LTC (primary y axis) and cumulative LTC (secondary y axis) as a function of phonon mean free path at 300 K. In (c) and (d), phonon modes are color-coded according to their relative particle and coherent contributions. Corresponding results for $Tl_2CdGeTe_4$ and $Tl_2HgSnSe_4$ are provided in Figs. S4 and S5 of the Supplemental Material [51].

transport (∼10% reduction in the in-plane LTC at 300 K). At 300 K, these materials exhibit ultralow in-plane LTCs of 0.32, 0.30, and 0.29 W m^{-1} K^{-1} for $Tl_2CdSnTe_4$, $Tl_2CdGeTe_4$, and $Tl_2HgSnSe_4$, while the corresponding cross-plane values of 0.55, 0.42, and 0.52 W m^{-1} K^{-1} indicate strong anisotropy, consistent with the directional dependence of phonon hybridization and rattling-induced scattering discussed above. The LTC exhibits a weak temperature dependence, following approximate power laws of $\kappa \propto T^{-0.67}$, $\kappa \propto T^{-0.65}$, and $\kappa \propto T^{-0.60}$ for in-plane transport in $Tl_2CdSnTe_4$, $Tl_2CdGeTe_4$, and $Tl_2HgSnSe_4$, respectively, deviating significantly from the stronger temperature scaling expected for purely three-phonon ($\kappa \propto T^{-1}$) or four-phonon ($\kappa \propto T^{-2}$) scattering.

The origin of this weak temperature dependence of LTC is understandable from the multichannel transport analysis shown in Fig. 3(b), which decomposes the in-plane thermal conductivity of $Tl_2CdSnTe_4$ into particlelike and coherent contributions (the corresponding results for $Tl_2CdGeTe_4$ and $Tl_2HgSnSe_4$ are provided in Figs. S4 and S5 in the SM [51]). At low temperatures, heat transport is dominated by the particle channel. With increasing temperature, however, the coherent contribution becomes increasingly more important, reaching approximately 32%, 38%, and 43% of the total in-plane LTC at 500 K in $Tl_2CdSnTe_4$, $Tl_2CdGeTe_4$, and $Tl_2HgSnSe_4$, respectively. Consequently, since the coherent channel contribution is glasslike and increases with temperature, the total LTC has a weak temperature dependence.

To elucidate the origin of the ultralow LTC, we analyze mode-resolved phonon transport for in-plane heat conduction in $Tl_2CdSnTe_4$, with the corresponding thermal conductivity accumulation and phonon mean free paths shown in Figs. 3(c) and 3(d) (see Figs. S4 and S5 in the SM [51] for $Tl_2CdGeTe_4$

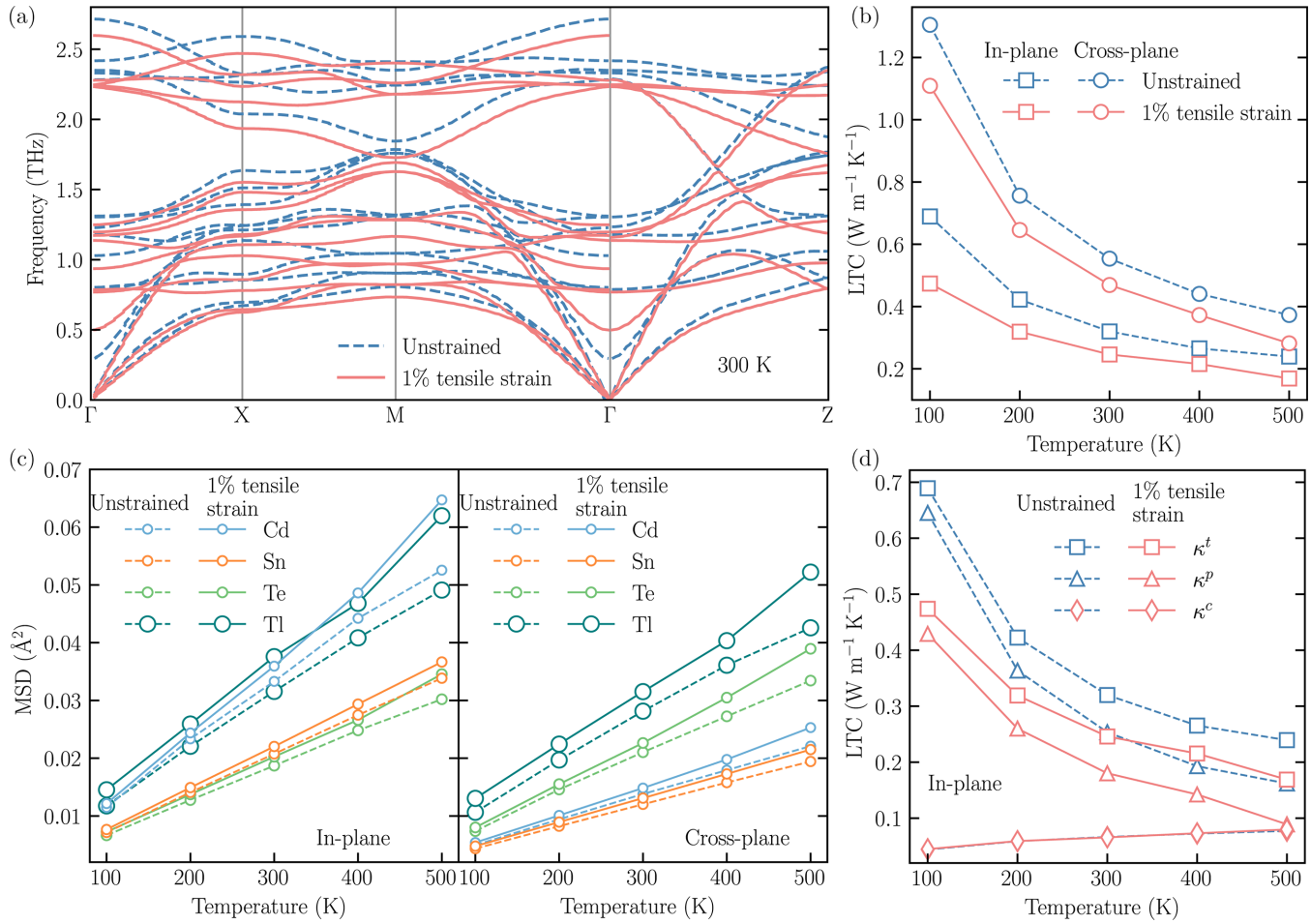


FIG. 4. Effect of 1% tensile strain on phonon properties and lattice thermal conductivity (LTC) of $Tl_2CdSnTe_4$. (a) Phonon dispersions at 300 K for unstrained and strained structures; for clarity, only frequencies up to 2.8 THz are shown (see Fig. S6 in the Supplemental Material [51] for the full frequency range). (b) Temperature-dependent LTC along the in-plane and cross-plane directions for unstrained and strained structures. (c) Direction-resolved mean-square displacements (MSDs) and (d) temperature-dependent decomposition of the total LTC κ^t into particle (κ^p) and coherent (κ^c) contributions.

and $Tl_2HgSnSe_4$). A large number of phonon modes appear with mean free paths below the Ioffe-Regel limit, indicating that the coherent-channel contribution could be significant in these materials. The results further suggest that heat transport is dominated by low-frequency phonons with frequencies below 2 THz in all three materials.

An interesting observation from the frequency-dependent LTC accumulation [Fig. 3(c)] is that nearly 75% of the particle-channel LTC contribution comes from modes with frequencies less than 1 THz, whereas these modes contribute only 20% to the coherent-channel LTC. This distinction allows the possibility of selectively suppressing particle-channel transport, while minimally affecting the coherent-channel contributions. Compared with conventional crystalline materials such as silicon, these modes exhibit exceptionally low phonon group velocities. Specifically, the in-plane longitudinal acoustic phonon group velocity in the long-wavelength limit is approximately 2.4 km s^{-1} in these materials, significantly smaller than the corresponding value in silicon (~8.6 km s^{-1}) [52].

In addition to their low velocities, these phonons exhibit strong anharmonicity, as reflected in the heat-capacity-weighted average Grüneisen parameters of 1.48, 1.54, and 1.53 for $Tl_2CdSnTe_4$, $Tl_2CdGeTe_4$, and $Tl_2HgSnSe_4$, respectively, compared to 1.02 in silicon [53]. The combined effect of reduced group velocities and enhanced anharmonic phonon-phonon interactions leads to intense scattering and ultrashort phonon mean free paths [Fig. 3(c)], with average values of 0.88, 0.74, and 0.68 nm, respectively, which are orders of magnitude smaller than those in silicon (~60 nm at 300 K). These factors act synergistically to suppress heat transport, giving rise to the ultralow LTC observed in these materials.

D. Strain engineering

Since the computationally relaxed lattice constants are underpredicted compared with the experimentally reported values by ~1% in both the in-plane and cross-plane directions, we examine the influence of tensile strain on LTC in $Tl_2CdSnTe_4$. Straining of the lattice is expected to weaken the rattler binding and thus enhance the anharmonicity in the system. The phonon dispersion of $Tl_2CdSnTe_4$ at 300 K under 1% tensile strain is compared with that of the relaxed structure

in Fig. 4(a) [for clarity, only modes up to 2.8 THz are shown in Fig. 4(a)].

The application of tensile strain softens the low-frequency phonon modes in $Tl_2CdSnTe_4$, leading to moderately decreased phonon group velocities. This softening is accompanied by an increase in vibrational amplitudes, particularly for Cd and Tl atoms [Fig. 4(c)], while Sn and Te atoms remain largely unaffected. In $Tl_2CdSnTe_4$ at 300 K, the in-plane MSDs of Tl atoms increase from 0.032 to 0.038 $Å^2$ under the applied strain. This enhancement reflects enhanced rattling behavior due to weakened Tl-framework bonding and is further evidenced by an increase in the mode-averaged Grüneisen parameter from 1.48 to 1.59 under 1% tensile strain.

The resulting impact on thermal transport is shown in Fig. 4(b), where the LTC under strain is reduced compared to the relaxed structure. The reduction is more pronounced in the in-plane direction, consistent with the anisotropic enhancement of Tl rattling. Decomposition of the in-plane LTC into particle and coherent contributions [Fig. 4(d)] reveals that this reduction is primarily driven by suppression of the particle channel, while the coherent contribution remains largely unchanged.

E. Utilizing design principles to lower LTC

As discussed above, the crystal structures of $Tl_2CdSnTe_4$ and $Tl_2CdGeTe_4$ are closely related to that of $Tl_2In_2Te_4$, in which the two In atoms are replaced by Cd and Sn/Ge, respectively. However, despite the comparable atomic masses of In, Cd, and Sn, the in-plane LTCs of $Tl_2CdSnTe_4$ and $Tl_2CdGeTe_4$ are approximately 25% lower than that of $Tl_2In_2Te_4$ obtained from similar first-principles calculations [23]. Furthermore, the similar in-plane thermal conductivities of $Tl_2CdSnTe_4$ and $Tl_2CdGeTe_4$ indicate that the overall reduction in LTC is largely insensitive to whether Sn or Ge occupies the framework site. Given that Sn and Ge possess similar valence states and chemical environments, we hypothesize that partial substitution between these two elements can introduce mass disorder and enhance phonon scattering without significantly perturbing interatomic interactions, thus potentially resulting in even lower LTC.

To test this hypothesis, we constructed a mixed composition based on the conventional unit cell of $Tl_2CdSnTe_4$, in which one of the two Sn atoms is replaced by Ge, yielding $Tl_4Cd_2SnGeTe_8$. As this represents a hypothetical structure, its thermodynamic and dynamical stabilities were assessed first. The calculated reaction enthalpy for decomposition into $Tl_2CdSnTe_4$ and $Tl_2CdGeTe_4$ is only 1.25 meV/atom, indicating that the mixed composition is thermodynamically stable. Phonon calculations reveal imaginary modes in the unstrained structure; however, these instabilities disappear under 1% tensile strain, confirming the dynamical stability of the strained configuration.

We therefore evaluate the LTC of the strained mixed compound and find a substantial reduction compared to the parent materials, with decreases of 30%–36% and 35%–45% in the in-plane and cross-plane directions, respectively [Fig. 5(a)]. Decomposition of LTC into the particle and coherent channel contributions [Fig. 5(b)] shows a slight enhancement of the coherent contribution; however, this effect is outweighed by a pronounced suppression of the particle channel. Analysis of phonon scattering [Figs. 5(c) and 5(d)] indicates that mass disorder enhances phonon-phonon scattering rates, leading to reduced phonon lifetimes and diminished particle-mediated heat transport. The inclusion of higher-order four-phonon scattering channels resulted in only a 6% reduction in the total LTC in the mixed compound, indicating that the three-phonon scattering events are sufficient to meaningfully describe the phonon lifetimes in these compounds. These results suggest that mass perturbation via isovalent substitution provides an effective design strategy for achieving significant reductions in LTC in these materials by selectively altering (reducing) only the particle contribution.

F. Ultralow-LTC materials

The discovery of materials with ultralow LTC is critical for applications in thermoelectric energy conversion and thermal insulation. While experimental exploration has historically relied on empirical design principles and trial-and-error approaches, advances in density functional theory have enabled predictive evaluation of LTC, providing a powerful framework for materials discovery. However, the high computational cost of such calculations continues to limit their applicability in large-scale screening efforts.

Recently, Al-Fahdi *et al.* [54] performed a high-throughput machine-learning-driven screening of ∼200 000 materials for extreme (high/low) LTC materials and obtained a dataset of 900 candidate materials with extreme LTC values. Subsequent first-principles validation yielded only 12 materials with LTC below 0.5 $W\,m^{-1}\,K^{-1}$, underscoring the difficulty of discovering intrinsically ultralow-LTC materials. Notably, none of these candidates contained Tl. In this context, the present work identifies three experimentally synthesized Tl-based compounds with intrinsically ultralow LTC. Experimental measurements on polycrystalline samples report direction-averaged thermal conductivities of ∼0.41 and ∼0.58 $W\,m^{-1}\,K^{-1}$ for $Tl_2CdSnTe_4$ and $Tl_2CdGeTe_4$, respectively [Fig. 3(a)]. Additionally, the screened materials are expected to be promising thermoelectric candidates, given that first-principles investigations of electronic transport properties in related Tl-based quaternary chalcogenides have reported favorable thermoelectric performance [55].

Furthermore, the ultralow-LTC values predicted for $Tl_2CdSnTe_4$, $Tl_2CdGeTe_4$, and $Tl_2HgSnSe_4$ are comparable to those reported for $AgTlI_2$ (∼0.25 $W\,m^{-1}\,K^{-1}$) [16]. Only a limited number of materials, such as $Bi_4O_4SeCl_2$ [10], $Cs_3Bi_2I_6Cl_3$ [56], $CsAg_5Te_3$ [57], and Ag_8SnSe_6 [58], are reported to exhibit lower thermal conductivities.

IV. CONCLUSIONS

In summary, we performed a comprehensive first-principles investigation of lattice thermal transport in the tetragonal chalcogenides $Tl_2CdSnTe_4$, $Tl_2CdGeTe_4$, and $Tl_2HgSnSe_4$ and demonstrated that these materials exhibit intrinsically ultralow LTC. Our analysis revealed that strong rattling dynamics of Tl atoms induce localization of low-frequency phonon modes, significantly suppressing heat-carrying acoustic phonons. Beyond conventional particlelike transport, we showed that coherent contributions become increasingly important at elevated temperatures,

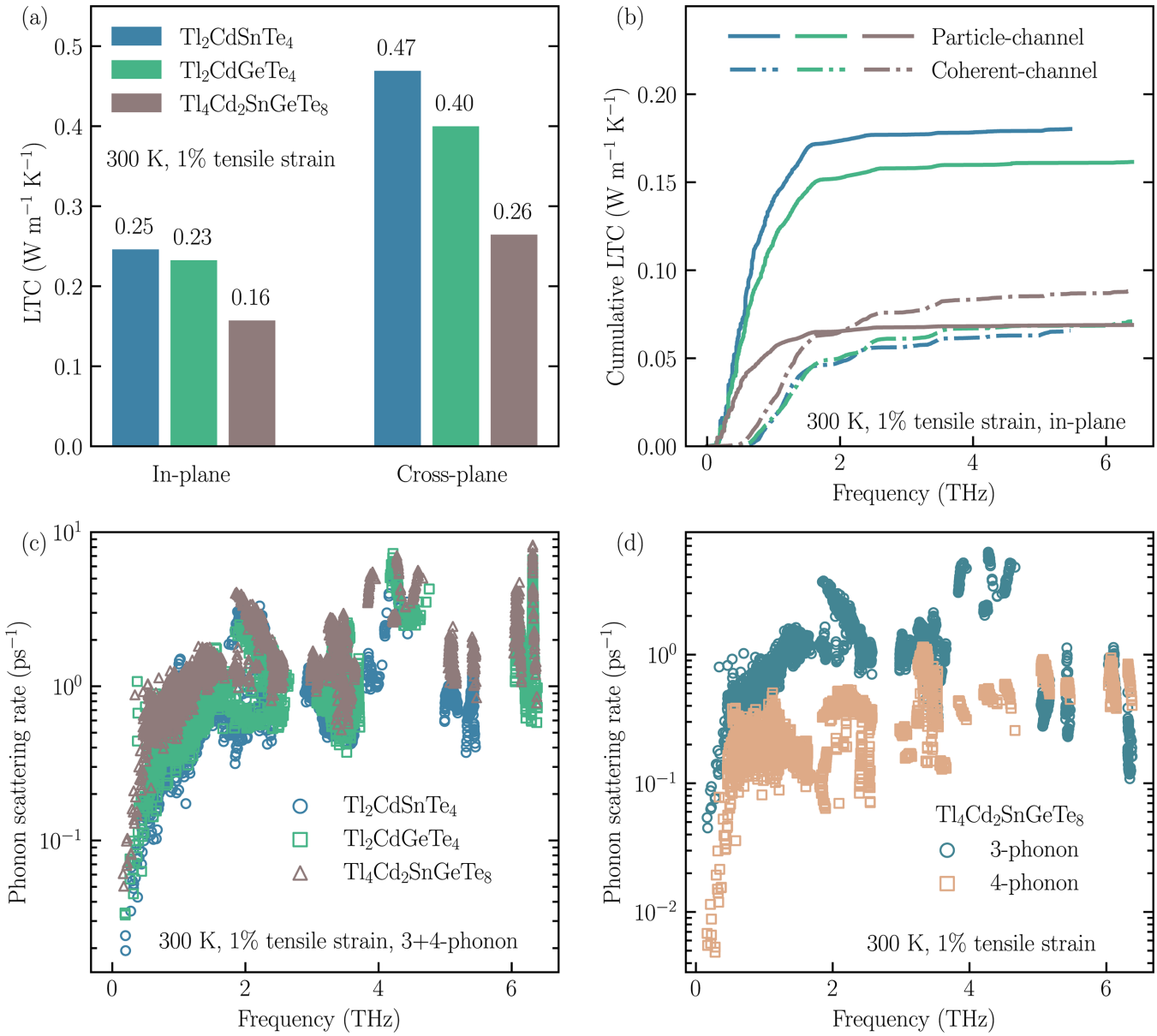


FIG. 5. Thermal transport properties of $Tl_4Cd_2SnGeTe_8$. (a) Comparison of in-plane and cross-plane lattice thermal conductivities (LTCs) of the mixed compound and its parent compounds ($Tl_2CdSnTe_4$ and $Tl_2CdGeTe_4$) at 300 K under 1% tensile strain. (b) Cumulative in-plane LTC as a function of phonon frequency for the mixed and parent compounds at 300 K. (c) Comparison of combined three- and four-phonon scattering rates for all three compounds. (d) Decomposition of scattering rates into three-phonon and four-phonon contributions for $Tl_4Cd_2SnGeTe_8$.

leading to a weak temperature dependence of LTC. We further demonstrated that tensile strain enhances anharmonicity and reduces LTC, primarily by suppressing the particle transport channel. In addition, we established mass perturbation via isovalent substitution as an effective strategy to further lower LTC, achieving substantial reductions in the mixed compound $Tl_4Cd_2SnGeTe_8$. These findings identify a class of experimentally accessible materials with ultralow LTC and provide general design principles (rattling-induced phonon localization, strain engineering, and mass disorder) for achieving strongly suppressed heat transport in crystalline solids.

ACKNOWLEDGMENTS

The authors acknowledge the financial support from the Advanced Research Grant (ARG), Anusandhan National Research Foundation (ANRF), India (Grant No. ANRF/ARG/2025/000326/PS). The calculations were carried out at the Praganak supercomputing facility at IIT Bombay and the PARAM Rudra (located at IIT Bombay, India) supercomputing facility provided by the Centre for Development of Advanced Computing (CDAC). N.V. acknowledges the financial support from the Prime Minister's Research Fellows (PMRF) scheme, Government of India.

DATA AVAILABILITY

The data that support the findings of this article are not publicly available upon publication because it is not technically feasible and/or the cost of preparing, depositing, and hosting the data would be prohibitive within the terms of this research project. The data are available from the authors upon reasonable request.

[1] G. Chen, M. Dresselhaus, G. Dresselhaus, J.-P. Fleurial, and T. Caillat, Recent developments in thermoelectric materials, Int. Mater. Rev. **48**, 45 (2003).

[2] G. J. Snyder and E. S. Toberer, Complex thermoelectric materials, Nat. Mater. **7**, 105 (2008).

[3] J. R. Sootsman, D. Y. Chung, and M. G. Kanatzidis, New and old concepts in thermoelectric materials, Angew. Chem. Int. Ed. **48**, 8616 (2009).

[4] J. M. Ziman, *Electrons and Phonons* (Clarendon, Oxford, 1960).

[5] J. Callaway, Model for lattice thermal conductivity at low temperatures, Phys. Rev. **113**, 1046 (1959).

[6] D. A. Broido, M. Malorny, G. Birner, N. Mingo, and D. A. Stewart, Intrinsic lattice thermal conductivity of semiconductors from first principles, Appl. Phys. Lett. **91**, 231922 (2007).

[7] M. N. Luckyanova, J. Garg, K. Esfarjani, A. Jandl, M. T. Bulsara, A. J. Schmidt, A. J. Minnich, S. Chen, M. S. Dresselhaus, Z. Ren, *et al.*, Coherent phonon heat conduction in superlattices, Science **338**, 936 (2012).

[8] R. Cheng, C. Wang, N. Ouyang, X. Shen, and Y. Chen, Strong crystalline thermal insulation induced by extended antibonding states, Nat. Commun. **16**, 7941 (2025).

[9] X. Qian, J. Zhou, and G. Chen, Phonon-engineered extreme thermal conductivity materials, Nat. Mater. **20**, 1188 (2021).

[10] Q. D. Gibson, T. Zhao, L. M. Daniels, H. C. Walker, R. Daou, S. Hébert, M. Zanella, M. S. Dyer, J. B. Claridge, B. Slater, *et al.*, Low thermal conductivity in a modular inorganic material with bonding anisotropy and mismatch, Science **373**, 1017 (2021).

[11] D. C. Schmitt, N. Haldolaarachchige, Y. Xiong, D. P. Young, R. Jin, and J. Y. Chan, Probing the lower limit of lattice thermal conductivity in an ordered extended solid: $Gd_{117}Co_{56}Sn_{112}$, a phonon glass–electron crystal system, J. Am. Chem. Soc. **134**, 5965 (2012).

[12] Y. Li, H. Guo, Z. Gao, W. Yan, H. He, B. Wei, J. Sun, J. Liu, C. Lu, Y. Nakamura, *et al.*, Dynamic local order and ultralow thermal conductivity of $Cs_2AgBiBr_6$, Nano Lett. **25**, 401 (2025).

[13] J. Zheng, C. Lin, C. Lin, G. Hautier, R. Guo, and B. Huang, Unravelling ultralow thermal conductivity in perovskite $Cs_2AgBiBr_6$: Dominant wave-like phonon tunnelling and strong anharmonicity, npj Comput. Mater. **10**, 30 (2024).

[14] P. Acharyya, T. Ghosh, K. Pal, K. Kundu, K. Singh Rana, J. Pandey, A. Soni, U. V. Waghmare, and K. Biswas, Intrinsically ultralow thermal conductivity in Ruddlesden–Popper 2D perovskite $Cs_2PbI_2Cl_2$: Localized anharmonic vibrations and dynamic octahedral distortions, J. Am. Chem. Soc. **142**, 15595 (2020).

[15] L.-D. Zhao, S.-H. Lo, Y. Zhang, H. Sun, G. Tan, C. Uher, C. Wolverton, V. P. Dravid, and M. G. Kanatzidis, Ultralow thermal conductivity and high thermoelectric figure of merit in SnSe crystals, Nature (London) **508**, 373 (2014).

[16] Z. Zeng, X. Shen, R. Cheng, O. Perez, N. Ouyang, Z. Fan, P. Lemoine, B. Raveau, E. Guilmeau, and Y. Chen, Pushing thermal conductivity to its lower limit in crystals with simple structures, Nat. Commun. **15**, 3007 (2024).

[17] M. Christensen, A. B. Abrahamsen, N. B. Christensen, F. Juranyi, N. H. Andersen, K. Lefmann, J. Andreasson, C. R. Bahl, and B. B. Iversen, Avoided crossing of rattler modes in thermoelectric materials, Nat. Mater. **7**, 811 (2008).

[18] G. S. Nolas, J. L. Cohn, and G. A. Slack, Effect of partial void filling on the lattice thermal conductivity of skutterudites, Phys. Rev. B **58**, 164 (1998).

[19] T. Tadano, Y. Gohda, and S. Tsuneyuki, Impact of rattlers on thermal conductivity of a thermoelectric clathrate: A first-principles study, Phys. Rev. Lett. **114**, 095501 (2015).

[20] T. Takabatake, K. Suekuni, T. Nakayama, and E. Kaneshita, Phonon-glass electron-crystal thermoelectric clathrates: Experiments and theory, Rev. Mod. Phys. **86**, 669 (2014).

[21] V. Keppens, D. Mandrus, B. C. Sales, B. Chakoumakos, P. Dai, R. Coldea, M. Maple, D. Gajewski, E. Freeman, and S. Bennington, Localized vibrational modes in metallic solids, Nature (London) **395**, 876 (1998).

[22] M. K. Jana, K. Pal, A. Warankar, P. Mandal, U. V. Waghmare, and K. Biswas, Intrinsic rattler-induced low thermal conductivity in Zintl type $TlInTe_2$, J. Am. Chem. Soc. **139**, 4350 (2017).

[23] K. Pal, Y. Xia, and C. Wolverton, Microscopic mechanism of unusual lattice thermal transport in $TlInTe_2$, npj Comput. Mater. **7**, 5 (2021).

[24] A. Jain, Multichannel thermal transport in crystalline Tl_3VSe_4, Phys. Rev. B **102**, 201201(R) (2020).

[25] M. Wu, Enamullah, and L. Huang, Unusual lattice thermal conductivity in the simple crystalline compounds $TlXTe_2$ (X = Ga, In), Phys. Rev. B **100**, 075207 (2019).

[26] S. Semwal, Y. Xia, C. Wolverton, and K. Pal, Concerted rattling-induced strong anharmonicity and phonon coherence lead to ultralow glasslike thermal conductivity in TlAgTe, Phys. Rev. B **112**, 214109 (2025).

[27] S. Mukhopadhyay, D. S. Parker, B. C. Sales, A. A. Puretzky, M. A. McGuire, and L. Lindsay, Two-channel model for ultralow thermal conductivity of crystalline Tl_3VSe_4, Science **360**, 1455 (2018).

[28] A. Jain, S. P. Ong, G. Hautier, W. Chen, W. D. Richards, S. Dacek, S. Cholia, D. Gunter, D. Skinner, G. Ceder, *et al.*, Commentary: The Materials Project: A materials genome approach to accelerating materials innovation, APL Mater. **1**, 011002 (2013).

[29] A. Jain, Y. Srivastava, A. G. Gokhale, N. Virakante, and H. L. Kagdada, Higher-order thermal transport theory for phonon thermal transport in semiconductors using lattice dynamics calculations and the Boltzmann transport equation, J. Indian Inst. Sci. (2025), doi:10.1007/s41745-025-00487-3.

[30] N. K. Ravichandran and D. Broido, Unified first-principles theory of thermal properties of insulators, Phys. Rev. B **98**, 085205 (2018).

[31] M. Simoncelli, N. Marzari, and F. Mauri, Unified theory of thermal transport in crystals and glasses, Nat. Phys. **15**, 809 (2019).

[32] T. Feng, L. Lindsay, and X. Ruan, Four-phonon scattering significantly reduces intrinsic thermal conductivity of solids, Phys. Rev. B **96**, 161201(R) (2017).

[33] M. Simoncelli, N. Marzari, and F. Mauri, Wigner formulation of thermal transport in solids, Phys. Rev. X **12**, 041011 (2022).

[34] A. J. McGaughey, A. Jain, H.-Y. Kim, and B. Fu, Phonon properties and thermal conductivity from first principles, lattice dynamics, and the Boltzmann transport equation, J. Appl. Phys. **125**, 011101 (2019).

[35] J. A. Reissland, *The Physics of Phonons* (Wiley, New York, 1973).

[36] W. Kohn and L. J. Sham, Self-consistent equations including exchange and correlation effects, Phys. Rev. **140**, A1133 (1965).

[37] R. G. Parr and W. Yang, *Density-Functional Theory of Atoms and Molecules* (Oxford University Press, Oxford, 1994).

[38] N. Virakante and A. Jain, Revisiting thermal transport in ThO_2 using higher-order thermal transport physics, Comput. Mater. Sci. **254**, 113882 (2025).

[39] P. Giannozzi, S. Baroni, N. Bonini, M. Calandra, R. Car, C. Cavazzoni, D. Ceresoli, G. L. Chiarotti, M. Cococcioni, I. Dabo, *et al.*, QUANTUM ESPRESSO: A modular and open-source software project for quantum simulations of materials, J. Phys.: Condens. Matter **21**, 395502 (2009).

[40] P. Giannozzi, O. Andreussi, T. Brumme, O. Bunau, M. B. Nardelli, M. Calandra, R. Car, C. Cavazzoni, D. Ceresoli, M. Cococcioni, *et al.*, Advanced capabilities for materials modelling with QUANTUM ESPRESSO, J. Phys.: Condens. Matter **29**, 465901 (2017).

[41] J. P. Perdew, A. Ruzsinszky, G. I. Csonka, O. A. Vydrov, G. E. Scuseria, L. A. Constantin, X. Zhou, and K. Burke, Restoring the density-gradient expansion for exchange in solids and surfaces, Phys. Rev. Lett. **100**, 136406 (2008).

[42] D. R. Hamann, Optimized norm-conserving Vanderbilt pseudopotentials, Phys. Rev. B **88**, 085117 (2013).

[43] Y. Srivastava, A. G. Gokhale, and A. Jain, Computational uncertainties in the prediction of lattice thermal conductivity of crystalline solids, Phys. Rev. B **112**, 195201 (2025).

[44] S. Baroni, S. De Gironcoli, A. Dal Corso, and P. Giannozzi, Phonons and related crystal properties from density-functional perturbation theory, Rev. Mod. Phys. **73**, 515 (2001).

[45] P. Giannozzi and S. Baroni, Density-functional perturbation theory, in *Handbook of Materials Modeling: Methods* (Springer, 2005), pp. 195–214.

[46] Z. Guo, P. Roy Chowdhury, Z. Han, Y. Sun, D. Feng, G. Lin, and X. Ruan, Fast and accurate machine learning prediction of phonon scattering rates and lattice thermal conductivity, npj Comput. Mater. **9**, 95 (2023).

[47] Y. Srivastava and A. Jain, Accelerating thermal conductivity prediction through machine-learning: Two orders of magnitude reduction in phonon-phonon scattering rates calculation, Mater. Today Phys. **41**, 101345 (2024).

[48] H. Matsumoto, K. Kurosaki, H. Muta, and S. Yamanaka, Systematic investigation of the thermoelectric properties of $TlMTe_2$ (M = Ga, In, or Tl), J. Appl. Phys. **104**, 073705 (2008).

[49] M. A. McGuire, T. J. Scheidemantel, J. V. Badding, and F. J. DiSalvo, Tl_2AXTe_4 (A = Cd, Hg, Mn; X = Ge, Sn): Crystal structure, electronic structure, and thermoelectric properties, Chem. Mater. **17**, 6186 (2005).

[50] M. Y. Mozolyuk, L. Piskach, A. Fedorchuk, I. Olekseyuk, and O. Parasyuk, Physico-chemical interaction in the $Tl_2Se{-}HgSe{-}D^{IV}Se_2$ systems (DIV–Si, Sn), Mater. Res. Bull. **47**, 3830 (2012).

[51] See Supplemental Material at http://link.aps.org/supplemental/10.1103/wh1q-59bc for details on the convergence of numerical parameters, additional figures for $Tl_2CdGeTe_4$ and $Tl_2HgSnSe_4$, and tables containing the complete list of computed lattice thermal conductivity values.

[52] H.-Y. Hao and H. J. Maris, Study of phonon dispersion in silicon and germanium at long wavelengths using picosecond ultrasonics, Phys. Rev. Lett. **84**, 5556 (2000).

[53] A. Jain and A. J. H. McGaughey, Thermal transport by phonons and electrons in aluminum, silver, and gold from first principles, Phys. Rev. B **93**, 081206(R) (2016).

[54] M. Al-Fahdi, R. Rurali, J. Hu, C. Wolverton, and M. Hu, Accelerated discovery of extreme lattice thermal conductivity by crystal graph attention networks and chemical bonding, npj Comput. Mater. **12**, 8 (2026).

[55] S. Hasan, S. San, K. Baral, N. Li, P. Rulis, and W.-Y. Ching, First-principles calculations of thermoelectric transport properties of quaternary and ternary bulk chalcogenide crystals, Materials **15**, 2843 (2022).

[56] P. Acharyya, T. Ghosh, K. Pal, K. S. Rana, M. Dutta, D. Swain, M. Etter, A. Soni, U. V. Waghmare, and K. Biswas, Glassy thermal conductivity in $Cs_3Bi_2I_6Cl_3$ single crystal, Nat. Commun. **13**, 5053 (2022).

[57] P.-F. Liu, X. Li, J. Li, J. Zhu, Z. Tong, M. Kofu, M. Nirei, J. Xu, W. Yin, F. Wang, *et al.*, Strong low-energy rattling modes enabled liquid-like ultralow thermal conductivity in a well-ordered solid, Natl. Sci. Rev. **11**, nwae216 (2024).

[58] Q. Ren, M. K. Gupta, M. Jin, J. Ding, J. Wu, Z. Chen, S. Lin, O. Fabelo, J. A. Rodríguez-Velamazán, M. Kofu, *et al.*, Extreme phonon anharmonicity underpins superionic diffusion and ultralow thermal conductivity in argyrodite Ag_8SnSe_6, Nat. Mater. **22**, 999 (2023).